Article:
Khodaparast, S, Sharratt, WN, Dalgliesh, RM et al. (1 more author) (2021) Growth of Myelin Figures from Parent Multilamellar Vesicles. Langmuir, 37 (42). pp. 12512-12517. ISSN 0743-7463

https://doi.org/10.1021/acs.langmuir.1c02464

Growth of myelin figures from parent multilamellar vesicles

Sepideh Khodaparast,*,† William N. Sharratt,‡ Robert M. Dalgliesh,¶ and João T. Cabral‡

†*Leeds Institute of Fluid Dynamics (LIFD), School of Mechanical Engineering, University of Leeds, LS2 9JT Leeds, UK.*

‡*Department of Chemical Engineering, Imperial College London, SW7 2AZ London, UK.*

¶*ISIS Neutron and Muon Source, Science and Technology Facilities Council, Rutherford Appleton Laboratory, OX11 0QX Didcot, UK.*

E-mail: s.khodaparast@leeds.ac.uk

Abstract

We examine the formation and growth of isolated myelin figures, microscale multilamellar tubules, from isotropic micellar solutions of an anionic surfactant. Upon cooling, surfactant micelles transform into multilamellar vesicles (MLVs), whose contact is found to trigger unidirectional growth of myelins. While the MLV diameter grows as $d_{MLV} \propto t^{1/2}$, myelins grow linearly in time $L_M \propto t^1$, with a fixed diameter. Combining time-resolved small angle neutron scattering (SANS) and optical microscopy, we demonstrate that the microscopic growth of spherical MLVs and cylindrical myelins stems from the same nanoscale molecular mechanism, namely the surfactant exchange from micelles into curved lamellar structures at a constant volumetric rate. This mechanism successfully describes the growth rate of (non-equilibrium) myelin figures based on a population balance at thermodynamic equilibrium.

Introduction

Synthetic amphiphilic molecules yield intricate self-assemblies, akin to natural phospholipid-based structures in biological membranes, hence providing opportunities for unravelling the complex dynamics and mimicking functionalities of living matter.[1] Elongated, multilamellar, concentric structures of surfactant bilayers, with repeat spacing of a few nm, have attracted special interest due to their resemblance to the striking tubular insulation which encapsulates the axon in neurons, called the myelin sheath.[2–5] Mimics of myelin figures are typically obtained by bringing a concentrated lamellar phase of a (synthetic or natural) surfactant or lipids in contact with a dilute aqueous solution, as shown in Fig. 1a. Such contact-dilution and immersion experiments provide a simple approach to examine the formation of myelins,[6–11] and several theories considering diffusion-driven processes[12–14] and water and surfactant influx mechanisms[12,15–18] have been proposed to describe the initiation and growth of myelin figures from planar lamellar structures. Resulting experimental observations and analyses are, however, impacted by the geometric, hydrodynamic and physicochemical complexities arising from the interaction and entanglement of closely packed lamellar tubes, significant hydration and surfactant gradients. Consequently, direct examination of the formation of isolated myelins under defined thermodynamic conditions has remained challenging.[8,19,20]

Here, we investigate the growth of isolated myelin figures from multilamellar vesicles (MLVs) of an anionic surfactant, Sodium Linear Alkylbenzene Sulfonate (NaLAS), formed spontaneously through a thermally-induced phase transformation,[21,22] see SI for more detail. In a contact-dilution experiment (Fig. 1a), a concentrated NaLAS lamellar phase Ⓐ is diluted in water, and yields a region of populated tubular lamellar structures Ⓑ at its interface, followed by an area covered with an isotropic micellar phase I Ⓒ. Both the planar and tubular lamellar structures appear birefringent and are easily distinguishable from the isotropic solution by polarised microscopy. The dilution occurs at a constant temperature, depicted by a horizontal arrow in Fig. 1a, corresponding to a transition from a mixed liquid

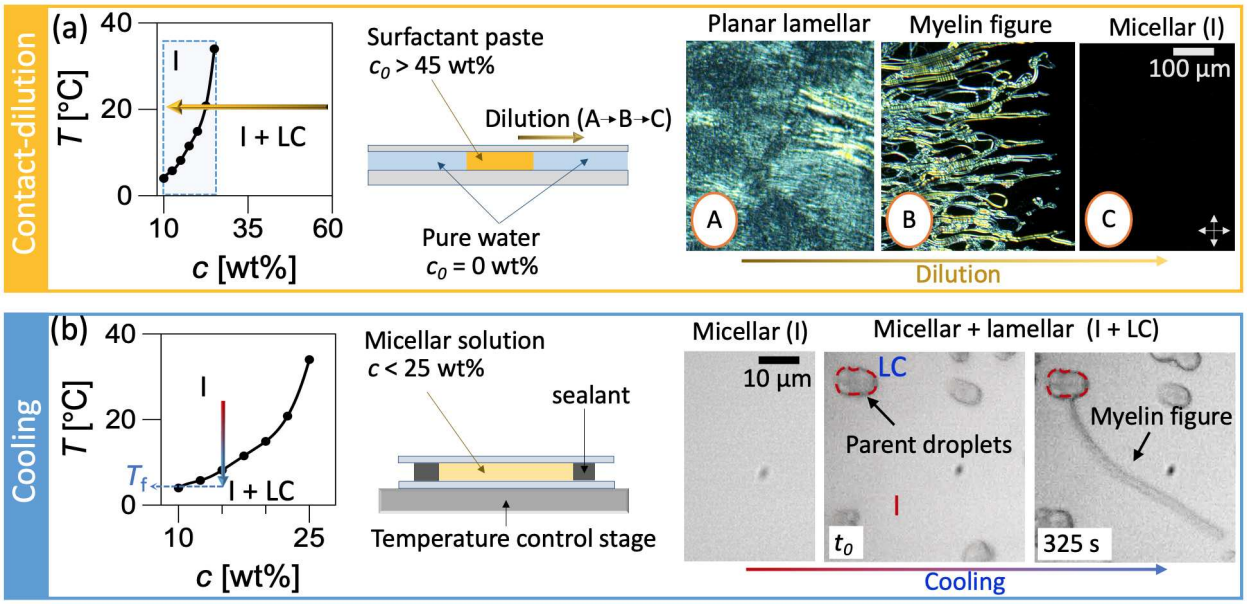

Figure 1: Growth of myelin figures of NaLAS surfactant in water induced by (a) contact-dilution and (b) cooling experiments. (a) A droplet of aqueous NaLAS mixture $c > 45$ wt% is exposed to pure water at room temperature; the temperature-concentration phase diagram depicts the dilution pathway. Cross-polarised microscopy images show the evolution of the planar lamellar phase Ⓐ as it develops tubular elongated features Ⓑ that extend towards the isotropic micellar phase Ⓒ. (b) A droplet of micellar solution of NaLAS is sandwiched between cover slips and sealed around its perimeter. Upon cooling at fixed concentration (here $c = 15$ wt%), a population of micelles transforms into a lamellar phase, spontaneously forming isolated multilamellar vesicles (MLVs), liquid crystalline (LC) droplets. Secondary nucleation on the surface of MLVs yield the formation of long slender tubular structures.

crystalline (here lamellar) and isotropic micellar phase to the dilute isotropic micellar phase. For a wide range of surfactant concentration, an inclined temperature-concentration phase boundary separates the micellar (I) and the mixed micellar and lamellar liquid crystalline (I + LC) phases, thus permitting the crossing of this phase boundary at *fixed* surfactant concentration through cooling, as shown in Fig. 1b. For more details of the equilibrium I and I + LC phases of NaLAS please refer to Khodaparast *et al.* (2019).[22]

Upon cooling a micellar solution of NaLAS at 10 wt% $< c <$ 25 wt%, a fraction of the NaLAS micelles[22] spontaneously forms MLVs, which coexist with the remaining micellar phase in the solution, see Fig. 1b and SI-video1. Under weak sub-cooling conditions (i.e. within ≤ 4 °C of the phase boundary), the secondary nucleation and growth of the concentric

LC phase, at the interface of an existing MLV, is found to initiate the growth of isolated myelin figures as shown in Fig. 1b, see SI-video2. In absence of external stimuli (concentration/temperature gradient or flow fields), these myelin figures are initiated at the point of discontinuity in the curvature generated at the junction of parent MLVs (Fig. 1b). As the myelins grow over time, the boundaries of the parent MLVs remain unchanged, in contrast to the continuously growing diameters of other MLVs in the solution (Fig. 1b). Similar growth of isolated long tubular filaments upon cooling has been occasionally observed in suspensions of liquid crystalline droplets.[16,23–26] In this work, we show that growth rate of such out-of-equilibrium tubular lamellar structures is controlled by the thermodynamic equilibrium of I + LC phases, and occurs through re-arrangement of surfactant molecules from the source micellar self-assemblies into the lamellar structures. We use NaLAS as a model system here as it permits spontaneous formation of MLVs in the absence of extra additives, however, growth mechanisms discussed here can explain dynamics of myelin growth in other systems of mixed surfactants and phospholipids.[16,17,23]

Materials and Methods

NaLAS was provided by P&G at 45 wt%. The concentrated solution was heated in an oven and homogenised before preparing the dilutions in deionised water. Please see the SI for more details on the chemical composition of NaLAS. Quiescent optical microscopy experiments (i.e., in the absence of flow) were performed by placing a 3 μL droplet of NaLAS solution between two cover slips, see Fig. 2. An annular sealant adhesive surrounded the droplet to minimise evaporation, thus concentration of surfactant c can be considered constant for these experiments. Linear cooling profiles were applied using a thermal stage (Linkam, LTS420) with rates ranging from 0.05 °C/min to 50 °C/min. Isothermal measurements were performed by quenching the sample at $\alpha_c = 50$ °C/min to the final temperature T_f and maintaining the final temperature T_f with an accuracy of 0.1 °C. Both polarised and

bright-field microscopy images were captured with an Olympus BX41M-LED microscope, using a 50X objective (Olympus, MPlanFL with NA 0.75) and a CMOS camera (Basler ace ac2040-90 uc), which provided an overall spatial resolution of 0.3 μm per pixel. Images were recorded at the rate of 1 frame per second.

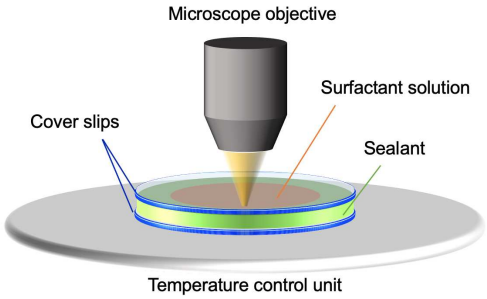

Figure 2: Schematic of the experimental setup used for OM measurements.

SANS experiments in various cooling cycles were performed on the LARMOR diffractometer (ISIS, UK) with a polychromatic neutron beam (with wavelength λ = 0.9-13.3 Å) and sample-to-detector distance of 4.1 m, yielding a momentum transfer range of approximately $0.005 < Q < 0.6$ Å^{-1}. See SI for more information on the experimental settings. No unexpected or unusually high safety hazards were encountered in the experiments.

Results and discussion

To investigate the microscopic growth and accompanying molecular assembly of the isotropic (micellar) and liquid crystalline (MLV and myelin) structures, we perform a series of time-resolved optical microscopy and small angle neutron scattering (SANS) experiments. Fig. 3a shows a characteristic isotropic (I) micellar solution (at T = 30 °C and NaLAS concentration c = 22.5 wt%) which is transparent in visible light and exhibits no birefringence; the corresponding SANS profile exhibits a broad peak (at $Q \simeq 0.1$ Å^{-1}), associated with the shape and structure factor of the charged ellipsoidal micelles.[22] Decreasing the temperature to T_f = 0 °C, corresponding to sub-cooling the solution by $\Delta T \simeq 20$ °C according to phase boundary in Fig. 1, results in the formation of two microscopically distinct LC patterns

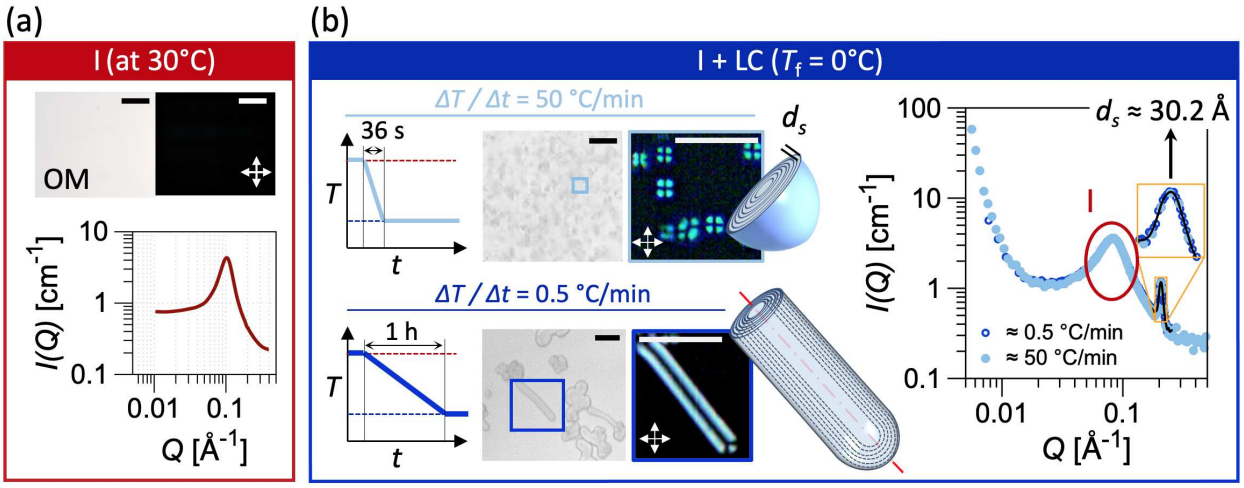

Figure 3: Micro and nanoscale analyses of the LC structures formed upon cooling the aqueous solution of 22.5 wt% NaLAS. (a) At 30 °C, micellar solution (phase I) appears transparent and black in optical and polarised microscopy, with a SANS profile characteristic of charged ellipsoidal micelles. (b) At 0 °C, relatively monodisperse multilamellar (birefringent) droplets nucleate when the solution is cooled rapidly (> 10°C/min), while mixed population of larger MLVs and myelin figures are obtained when the solution is cooled slowly (< 1°C/min). SANS measurements of both solutions at 0 °C exhibit a clear Bragg peak located at $Q \approx 0.208$ Å^{-1}, corresponding to bilayer spacing of $d_s \approx 30.2$ Å. The lamellar LC phase coexcists with the micellar phase (phase I + LC), manifested by the micellar scattering profile with peak at $Q \approx 0.08$ Å^{-1}. Scale bars correspond to 10 μm. Equilibrium saturation temperature of the solution at 0 °C is approximately 21 °C, providing $T_s - T_f = 21$ °C.

shown in Fig. 3b: (i) at high cooling rates (here 50 °C/min), a large number of relatively monodisperse microscale LC droplets appear, with birefringence indicative of concentric multilayered vesicles (MLVs). Real-space images of the internal structure of the MLVs are captured using transmission electron microscopy, see Fig. S2. Rapid cooling allows bypassing the intermediate equilibrium states, and MLVs are formed after the final temperature (here 0 °C) has been reached; (ii) at low cooling rates ($\Delta T/\Delta t \leq 1$ °C/min), a small number of isolated, large MLVs form initially, and subsequently become sites for secondary nucleation. A relatively large population of myelin figures form at the location of non-matching curvatures of the initial and secondary droplets. Slow cooling yields continuous formation and growth of MLVs and myelin figures within the solution exposed to constant temperature drop at the rate of $\frac{\Delta T}{\Delta t} = 0.5$ °C/min. While the two LC structures obtained in (i) and (ii) are microscopically distinct, the nanoscale SANS scattering patterns obtained at similar

conditions are effectively identical with an overlapping Bragg peak position, associated with the bilayer d-spacing of $d_s \approx 30.2$ Å (Fig. 3b). In both cases, the LC phase coexists with the isotropic micellar phase (I) whose scattering profile spans across the intermediate Q range. SANS measurements at different cooling rates, demonstrate that within the coexisting I + LC region, an equilibrium population ratio is established between the I and LC phases, which is solely determined by the final equilibrium temperature T_f and surfactant concentration c, regardless of the thermal history and cooling pathway.[22] Furthermore, formation of larger MLVs and myelin figures in slow cooling experiments, suggests that weak sub-cooling is essential to achieve polydispersity and myelin growth, see Fig. S3. We note that the scattering intensities vary slightly in the low-Q region, as expected from the formation of distinct microscale aggregates in slow and fast cooling tests.

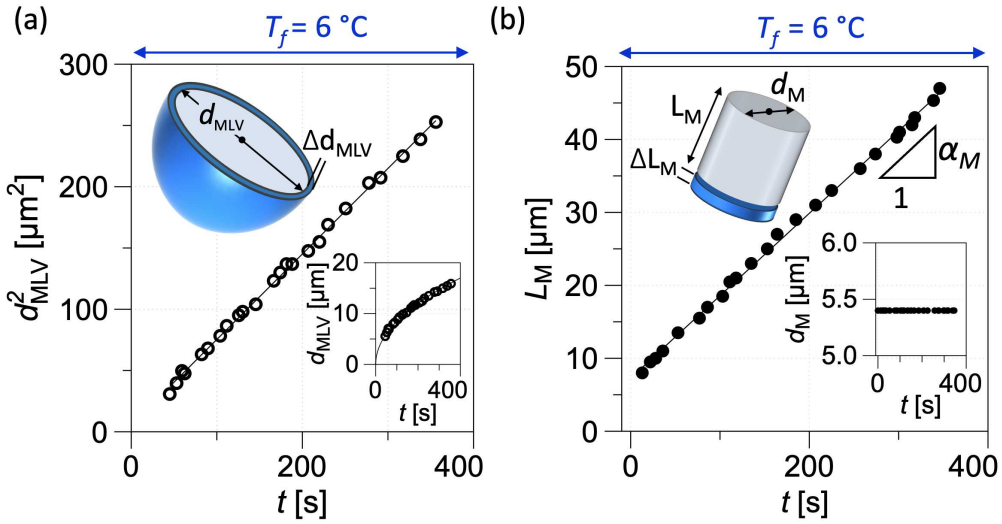

Figure 4: Isothermal growth of MLVs and myelin figures at $T_f = 6$ °C ($T_s - T_f = 2$ °C) for $c = 15$ wt%. (a) The diameter of the MLVs (d_{MLV}) increases with $t^{1/2}$, $d^2_{MLV} \propto t$. MLVs grow through accumulation of thin bilayer shells. (b) Myelin figures grow linearly in length L_M through accumulation of thin discs, maintaining an unchanged diameter (here $d_M = 5.4 \pm 0.3$ μm).

We next report on isothermal experiments in which the micellar solution is rapidly quenched (at 50 °C/min) to reach a series of temperature T_f and held isothermally. T_f is chosen to be close to the phase boundary to provide weak sub-cooling and larger population of myelin figures. Isothermal experiments allow us to eliminate thermal diffusion as the

potential driving mechanism for growth of myelins in our system.[13] The geometric evolution of the myelins and MLVs with time is examined as a means to elucidate the underpinning growth mechanism. Most previous studies reported power laws $L_M \propto t^{0.5}$ for radial ensemble growth of myelin figures in contact dilution experiments.[8,9,15,27] Notable exceptions to this trend include the linear growth $L_M \propto t$ of individual myelins observed by cooling a mixed surfactant solution reported by Toquer *et al.*,[23] and in droplet drying experiments reported by Zou and Nagel.[16,17] In our isothermal experiments at fixed surfactant concentration, we find that while the diameter of MLVs grows with square root of time, $d_{MLV} \propto t^{0.5}$, the length of myelin figures follows $L_M \propto t^1$ with an effectively unchanged base diameter d_M (Fig. 4). This scaling holds for considerable time, close to the point at which temperature-dependent population balance between I and LC phases is reached. The distinct evolution of the spherical MLVs and cylindrical myelins, with an *identical* bilayer structure and thermodynamic driving force, suggests that the dimensionality of the microscale geometry of the LC structure determine the scaling with time.

Previous time-resolved small angle scattering analyses have suggested that spherical MLVs grow through accumulation of effectively two-dimensional uni-lamellar shells,[22,28–30] here yielding an outward radial growth of the droplets that is clearly observable in optical analyses. The volumetric growth unit of MLVs is thus estimated by $\Delta V_{MLV} = \pi d_{MLV,t}^2 d_s$ as a function of time, where $d_{MLV,t}$ is the time-dependent MLV diameter and d_s is the constant shell thickness, set by the bilayer spacing (Fig. 4a). Myelin figures, however, maintain their initial cross-sectional diameter unchanged, while growing one-dimensionally in length. Therefore, volumetric growth unit of myelins at any time instance yields $\Delta V_M = \frac{\pi}{4} d_M^2 \Delta L_{M,t}$, highlighted in bright blue color in Fig. 4b, where $\Delta L_{M,t}$ is the axial unit growth. Our experimental data presented in Fig. 4 show that the rates of increase for $d_{MLV,t}^2$ and $\Delta L_{M,t}$ are constant in time, thus suggesting that growth of both structures is affected by a constant volumetric inflow, *i.e.* $\frac{\Delta V}{\Delta t}$ is constant. The linear growth of myelin figures observed here, suggests a cross-sectional growth through the root,[16] as opposed to the growth via

absorption of surfactant on the external cylindrical body of the structure suggested by Pratibha and Madhusudana that yields an exponential growth.[25] Growth of both multilamellar vesicles and myelin figures induced by cooling is reversible through heating the solution. Upon heating, myelins dissolve back and form micelles. During the course of dissolution, the length of myelins decreases linearly until until reaching $L_M = 0$ at the contact point with the original parent droplets. The linear rate of growth/dissolution is a function of cooling/heating rate and will be discussed later; i.e. higher rate of cooling/heating yields faster growth/dissolution for a given cross-sectional area of myelin, see an example in Fig. 5.

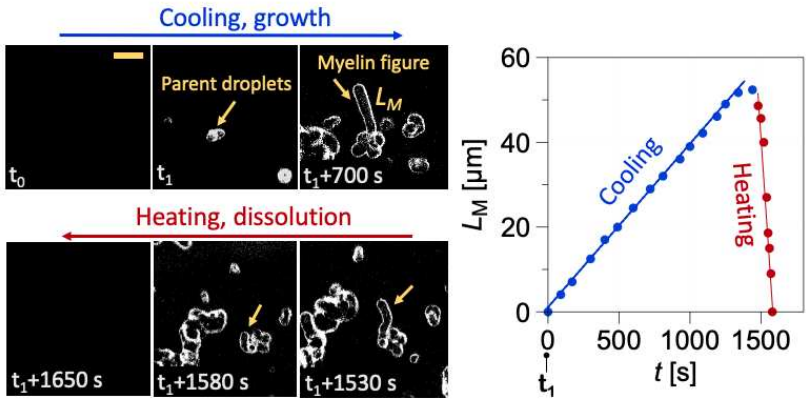

Figure 5: Linear growth and dissolution of myelin figures in an aqueous solution of NaLAS at $c = 15$ wt%. Cooling and heating cycles are performed at 0.1 °C/min and 1 °C/min, thus yielding various rates of growth/dissolution. Scale bar corresponds to 10 μm.

The growth of MLVs and myelin figures occurs by promoting a conversion from the micellar to the lamellar phase upon cooling, which can be quantified by time-resolved SANS, see an example in Fig. 6a. Micellar volume fractions are extracted from model fits to the mid-Q region of the scattering data and used to estimate the volumetric concentration of the micellar phase in the mixed micellar and liquid crystalline phase, see an example fit in Fig. 6b. See more details of the model used to obtain the micellar fit in the SI. Monitoring the evolution of the scattering profile arising from the micellar and lamellar structures, the volumetric concentration loss of the micellar phase Φ_I during this transformation can be readily computed, as shown in Fig. 6c. Significantly, the loss in volumetric concentration of

micelles is largely linear in time, corroborating that a constant volumetric inflow of surfactant controls the growth rate of both MLVs and myelin figures. All quantitative data on the growth of myelin figures and MLVs presented here are collected during the linear conversion period. Governed by molecular diffusion, the linear conversion trend slows down as the solution approaches equilibrium (Fig. 6c). See the SI (Fig. S4) for comparison between growth rates at the main linear and late stage of the material conversion. The magnitude of the final equilibrium volumetric concentration of the micellar phase is defined by T_f, regardless of the cooling history. As discussed earlier, rapid cooling allows monitoring the transformations that occur at the final temperature T_f, as the result of solution exposure to total $\Delta\Phi_I$. Expectedly, $\Delta\Phi_I$ obtained in isothermal experiments increases at lower final equilibrium temperature T_f, see Fig. 6d.

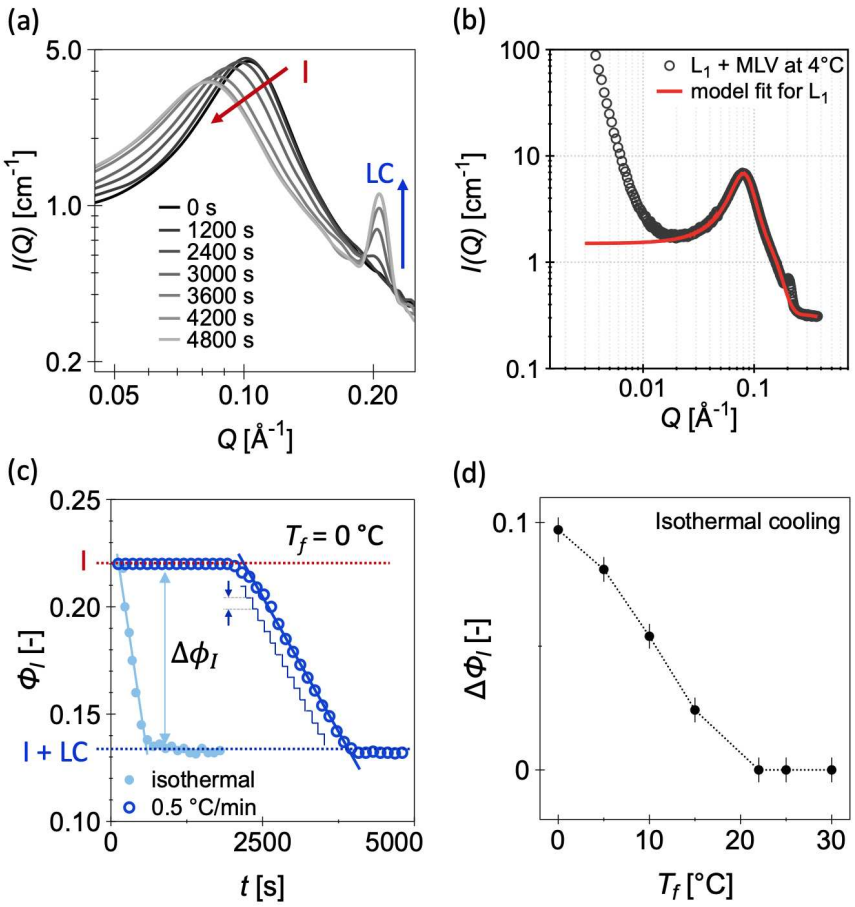

Figure 6: Conversion from the micellar to the LC phase upon cooling. (a) Time-resolved SANS scattering data for 22.5 wt% NaLAS solution, cooled from 30 °C down to 0 °C at 0.5 °C/min. (b) An example of the fit obtained for the micellar phase coexisting with the LC phase. The micellar fit is used to estimate the volumetric concentration of the micelles. (c) The volumetric concentration of micelles Φ_I decreases linearly in time upon phase transformation affected by cooling. Horizontal red/blue dotted lines depict equilibrium volumetric concentration of micelles in the I/I+LC phases at 30 °C/0 °C. $\Delta\Phi_I$ is the difference between the equilibrium volumetric concentration of micelles. (d) In isothermal experiments, $\Delta\Phi_I$ decreases continuously as the final equilibrium temperature T_f increases, until purely micellar phase is reached.

The constant volumetric growth of myelins imposes a reduction in the myelin growth rate α_M (defined as the proportionality constant, $L_M \equiv \alpha_M t$) as the myelin base diameter d_M increases, at given c and T_f. Isothermal measurements presented in Fig. 7a show not only a reduction in α_M for thicker myelin figures, but also a clear power-law correlation $\alpha_M \propto d_M^{-2}$ as expected from the volumetric argument above. In line with SANS analyses, the myelin

growth rate increases as deeper levels of sub-cooling (larger $T_s - T_f$ and $\Delta\Phi_I$) are reached, see the inset in Fig. 7a. In contrast, slow cooling rates impose gradual transformation through exposure to a series of relatively weaker sub-cooling and $\Delta\Phi_I$ (Fig. 6c). Under such conditions, the rate of transfer from the micellar to the lamellar phase is impacted by the rate of cooling. Optical microscopy measurements of myelin growth during continuous cooling at constant rates (Fig. 7b) show that increasing the cooling rate by an order of magnitude leads to similar enhancement in growth rate of myelin figures. Similar to isothermal measurements, the myelin growth rate at a fixed concentration inversely scales with d_M^2 (Fig. 7b).

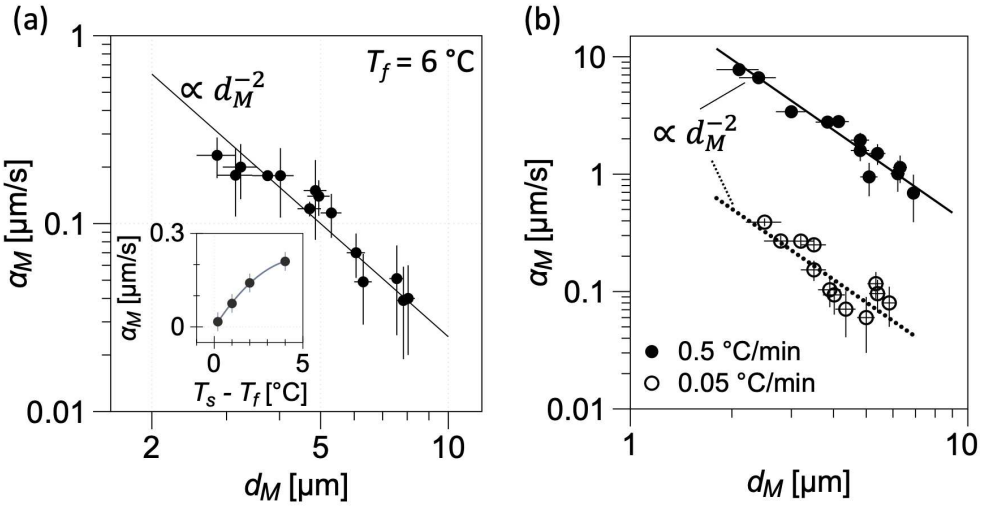

Figure 7: Rate of linear growth in the length of myelin figures obtained under isothermal and continuous cooling conditions. (a) The rate of the linear temporal growth of the myelin figures α_M at a given thermodynamic state ($c = 15$ wt%, $T_f = 6$ °C) is inversely proportional to d_M^2. Reducing T_f in independent isothermal experiments, accelerates the growth of myelin figures, plotted versus $T_s - T_f$, where T_s is the saturation temperature at $c = 15$ wt%. (b) α_M obtained in slow cooling experiments performed at 0.05 and 0.5 °C/min. Higher cooling rates result in faster growth of myelin figures, while $\alpha_M \propto d_M^{-2}$ for all measurements.

In conclusion, we identify the transfer of surfactants molecules, from micelles to lamellar structures, as the mechanism governing the temporal growth of both MLVs and myelin figures. While myelins are non-equilibrium structures,[16] we find that their growth kinetics can be described by a simple geometric argument and finely tuned by the thermodynamic driving force between equilibrium states, here traversed by temperature changes. Linear elongation of myelin figures with a constant cross-sectional diameter suggests that they grow

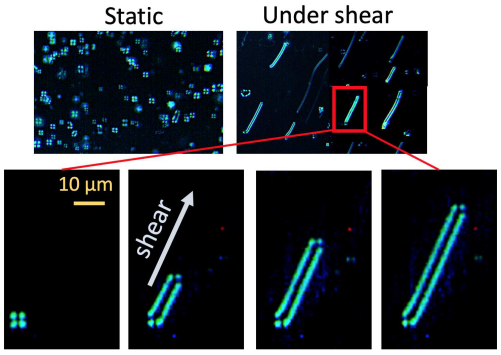

Figure 8: Growth of myelin figures from MLVs, exposed to shear stress at a constant temperature. Images are captured for a solution of $c = 17$ wt% at $T_f = 10$ °C.

via an inflow of surfactant molecules through their root,[16] as opposed to absorption on their cylindrical interface.[25] Our measurements indicate no significant bilayer spacing change during myelin growth, and therefore the mechanism proposed[19] for myelin growth from planar lamellar structures based on compensation in curvature energy is not applicable to our system. The question of what initiates the growth of the isolated myelin figures observed here remains to be answered through further investigations. In static conditions, myelins figures in our system grow at the non-matching curvature contact points of primary and secondary MLV droplets. By contrast, under hydrodynamic shear stress, we find myelins to spontaneously grow from single droplets maintaining the parent droplet diameter, thus acquiring hemispherical caps on both ends, see Fig. 8. The growth of myelin figures affected by hydrodynamic shear follows a similar linear trend with time, approving the validity of the current discussions for externally imposed directional growth of such objects. Simultaneous thermal and hydrodynamic manipulation of MLV forming amphiphilic systems in confinement thus offers new routes for fabrication of complex soft slender bodies with well-controlled dimensions and deserves dedicated studies in the future. Overall, our findings demonstrate that precise knowledge of thermodynamic equilibrium phases in solutions of amphiphilic molecules, and associated transition kinetics, is essential to mechanistically describe and control the formation and dynamics of these fascinating self-assemblies.

Acknowledgement

SK is partially supported by The Wellcome Trust Institutional Strategic Support Fund (ISSF) from University of Leeds. JTC thanks the Royal Academy of Engineering (RAEng, UK) and P&G for funding a research chair, and P&G for kindly providing NaLAS surfactant samples. Experiments at the ISIS Neutron and Muon Source were supported by a beam-time allocation RB1820374 from the Science and Technology Facilities Council. This work benefited from the use of the SasView application, originally developed under NSF Award DMR-0520547. SasView also contains code developed with funding from the EU Horizon 2020 programme under the SINE2020 project Grant No 654000.

Supporting Information Available

Supporting Information. Videos of (1) the growth and dissolution of MLV droplets and (2) growth of myline figures from MLVs. Supplemantary Material providing information on the chemical structure of NaLAS, growth and structures of MLVs and myelin figures.

References

(1) Hamley, I. W.; Castelletto, V. Biological soft materials. *Angew Chem Int Ed Engl* **2007**, *46*, 4442–4455.

(2) Bangham, A.; Standish, M.; Watkins, J. Diffusion of univalent ions across the lamellae of swollen phospholipids. *J Mol Biol* **1965**, *13*, 238–IN27.

(3) Szoka, F. J.; Papahadjopoulos, D. Comparative properties and methods of preparation of lipid vesicles (liposomes). *Annu Rev Biophys Bioeng* **1980**, *9*, 467–508.

(4) Hargreaves, W. R.; Deamer, D. W. *Biochemistry*; American Chemical Society, 1978; Vol. 17; pp 3759–3768.

(5) Boullerne, A. I. The history of myelin. *Exp Neurol* **2016**, *283*, 431–445.

(6) Sakurai, I.; Suzuki, T.; Sakurai, S. Cross-sectional view of myelin figures. *Biochimica et Biophysica Acta (BBA) - Biomembranes* **1989**, *985*, 101 – 105.

(7) Buchanan, M.; Arrault, J.; Cates, M. E. Swelling and Dissolution of Lamellar Phases: Role of Bilayer Organization. *Langmuir* **1998**, *14*, 7371–7377.

(8) Dave, H.; Surve, M.; Manohar, C.; Bellare, J. Myelin growth and initial dynamics. *J Colloid Interf Sci* **2003**, *264*, 76–81.

(9) Reissig, L.; Fairhurst, D. J.; Leng, J.; Cates, M. E.; Mount, A. R.; Egelhaaf, S. U. Three-dimensional structure and growth of myelins. *Langmuir* **2010**, *26*, 15192–15199.

(10) Bhatia, T.; Hatwalne, Y.; Madhusudana, N. V. Tubular growth and bead formation in the lyotropic lamellar phase of a lipid. *Soft Matter* **2015**, *11*, 5641–5646.

(11) Benkowska-Biernacka, D.; Smalyukh, I. I.; Matczyszyn, K. Morphology of Lyotropic Myelin Figures Stained with a Fluorescent Dye. *J. Phys. Chem. B* **2020**, *124*, 11974–11979.

(12) Sakurai, I.; Kawamura, Y. Growth mechanism of myelin figures of phosphatidylcholine. *Biochim Biophys Acta* **1984**, *777*, 347–351.

(13) Naito, H.; Okuda, M.; Zhong-can, O.-Y. Pattern formation and instability of smectic-A filaments grown from an isotropic phase. *Phys. Rev. E* **1997**, *55*, 1655–1659.

(14) Chaieb, S.; Sutin, J. Growth of myelin figures made of water soluble surfactant. 1st Annual International IEEE-EMBS Special Topic Conference on Microtechnologies in Medicine and Biology. Proceedings (Cat. No.00EX451). 2000; pp 345–348.

(15) Buchanan, M.; Egelhaaf, S. U.; Cates, M. E. Dynamics of Interface Instabilities in Nonionic Lamellar Phases. *Langmuir* **2000**, *16*, 3718–3726.

(16) Zou, L.-N.; Nagel, S. R. Stability and growth of single myelin figures. *Phys Rev Lett* **2006**, *96*, 138301.

(17) Zou, L.-N. Myelin figures: The buckling and flow of wet soap. *Phys. Rev. E* **2009**, *79*, 061502.

(18) Bhatia, T. Tubules, beads, discs and junctions – Morphologies and dynamics of dispersed multilamellar lipid phases in excess water. *Journal of Colloid and Interface Science* **2021**, *584*, 706–713.

(19) Huang, J. R.; Zou, L. N.; Witten, T. A. Confined multilamellae prefer cylindrical morphology. *The European Phys J E* **2005**, *18*, 279–285.

(20) Panahi, M. A.; Tahmasebi, Z.; Abbasian, V.; Amiri, M.; Moradi, A.-R. Role of pH level on the morphology and growth rate of myelin figures. *Biomed. Opt. Express* **2020**, *11*, 5565–5574.

(21) Stewart, J. A.; Saiani, A.; Bayly, A.; Tiddy, G. J. T. The phase behaviour of lyotropic liquid crystals in linear alkylbenzene sulphonate (LAS) systems. *Colloids Surf A* **2009**, *338*, 155 – 161.

(22) Khodaparast, S.; Sharratt, W.; Wang, H.; Robles, E. S.; Dalgliesh, R.; Cabral, J. T. Spontaneous formation of multilamellar vesicles from aqueous micellar solutions of sodium linear alkylbenzene sulfonate (NaLAS). *J. Colloid Interf. Sci.* **2019**, *546*, 221 – 230.

(23) Toquer, G.; Phou, T.; Monge, S.; Grimaldi, A.; Nobili, M.; Blanc, C. Colloidal Shape Controlled by Molecular Adsorption at Liquid Crystal Interfaces. *J. Phys. Chem. B* **2008**, *112*, 4157–4160.

(24) Blanc, C. Interplay between growth mechanisms and elasticity in liquid crystalline nuclei. *Prog. Theor. Phys.* **2008**, *175*, 93–102.

(25) Pratibha, R.; Madhusudana, N. V. Cylindrical growth of smectic A liquid crystals from the isotropic phase in some binary mixtures. *Journal de Physique II* **1992**, *2*, 383–400.

(26) Peddireddy, K.; Čopar, S.; Le, K. V.; Muševič, I.; Bahr, C.; Jampani, V. S. R. Self-shaping liquid crystal droplets by balancing bulk elasticity and interfacial tension. *Proceedings of the National Academy of Sciences* **2021**, *118*, e2011174118.

(27) Peddireddy, K.; Kumar, P.; Thutupalli, S.; Herminghaus, S.; Bahr, C. Myelin Structures Formed by Thermotropic Smectic Liquid Crystals. *Langmuir* **2013**, *29*, 15682–15688.

(28) Bressel, K.; Muthig, M.; Prevost, S.; Gummel, J.; Narayanan, T.; Gradzielski, M. Shaping Vesicles–Controlling Size and Stability by Admixture of Amphiphilic Copolymer. *ACS Nano* **2012**, *6*, 5858–5865, PMID: 22713309.

(29) Gummel, J.; Sztucki, M.; Narayanan, T.; Gradzielski, M. Concentration dependent pathways in spontaneous self-assembly of unilamellar vesicles. *Soft Matter* **2011**, *7*, 5731–5738.

(30) Landman, J.; Ouhajji, S.; Prévost, S.; Narayanan, T.; Groenewold, J.; Philipse, A. P.; Kegel, W. K.; Petukhov, A. V. Inward growth by nucleation: Multiscale self-assembly of ordered membranes. *Sci. Adv.* **2018**, *4*, eaat1817.

Graphical TOC Entry